Revised Limits on ISO 19905-1 Tubular Member Limiting Diameter to Thickness Ratios given Water Depth

P.A. Frieze*
PAFA Consulting Engineers
UK
** corresponding author: pafrieze@pafa-consulting-engineers.co.uk*

ABSTRACT
Changes have been made to the ISO 19902 tubular member strength formulations on which ISO 19905-1 Table A.12.5-1 is based and more are proposed. The paper examines the changes in detail and identifies those now controlling the tabulated values. They are used to revise the relationship between limiting water depth and diameter to thickness and to recommend an updated Table A.12.5-1. The revision relaxes the present limits by 11%.

KEY WORDS: Jack-ups, tubular members, strength formulations, limiting water depths.

INTRODUCTION

ISO 19905-1 Table A.12.5-1 provides tubular member limiting diameter to thickness (D/t) ratios given water depth *d*. These values were derived in 2002 [1] using the strength formulations in a draft of ISO 19902:2007 Fixed steel offshore structures. Bending was found to be more influential than axial compression. This led to the decision to use a 10% reduction in bending strength in the presence of hydrostatic pressure as the basis for the tabulated D/t values.

In ISO 19902:2020, the interaction formulae between local axial tension/compression and bending were improved by replacing the original linear interaction by the cosine form. This also reduced the conservatism in the local axial/bending strength formulations when combined with hydrostatic pressure. However, no attempt was made to assess the implications for the D/t limits in Table A.12.5-1.

Inadequacies and inconsistencies in the ISO 19902 formulations for the effect of hydrostatic pressure on bending strength had already been highlighted in [2] which were further underlined in [3] even after accounting for the 2020 changes to ISO 19902. Proposals to overcome these were developed [4] which are now expected to be included in the next edition of ISO 19902.

The paper describes the advances reported in [4] which are then used to derive new water depth limits for use in Table A.12.5-1.

ORIGINAL ISO 19902 LOCAL STRENGTH FORMULATIONS

The ISO 19902:2007 equations governing tubular member strength in the presence of hydrostatic pressure are shown in Equations (1) to (3). They are presented here for a single plane of bending/buckling for consistency with the test data with which they are compared – see ISO 19902 Clause A.13 and below:

$$\frac{\gamma_{R,t}\sigma_{t,c}}{f_{t,h}} + \frac{\gamma_{R,b}\sigma_b}{f_{b,h}} \leq 1.0 \tag{1}$$

$$\frac{\gamma_{R,c}\sigma_{c,c}}{f_{yc}} + \frac{\gamma_{R,b}\sigma_b}{f_{b,h}} \leq 1.0 \tag{2}$$

$$\frac{\gamma_{R,c}\sigma_c}{f_{c,h}} + \frac{\gamma_{R,b}}{f_{b,h}} \frac{C_m\sigma_b}{1-\sigma_c/f_e} \leq 1.0 \tag{3}$$

in which

$\sigma_{t,c}$	axial tensile stress due to factored actions including capped-end actions,
$f_{t,h}$	tensile strength in the presence of hydrostatic pressure,
$\sigma_{c,c}$, σ_c	axial compressive stress due to factored actions including and excluding capped-end actions, respectively,

f_{yc}, $f_{c,h}$	local buckling strength, column buckling strength in presence of hydrostatic pressure,
σ_b	bending stress due to factored actions,
C_m	moment reduction factor, taken as 1.0 when interpreting test results,
f_e	Euler buckling stress,
$f_{b,h}$	bending strength in the presence of hydrostatic pressure,
$\gamma_{R,t}$, $\gamma_{R,c}$, $\gamma_{R,b}$	partial resistance factors for tension, compression and bending, respectively.

The tensile and bending strengths in the presence of pressure, $f_{t,h}$ and $f_{b,h}$, were derived from the modified Beltrami-Haigh biaxial yield function – see Equation (4) and Figure 1 (η is the modification):

$$\left(\frac{\sigma_a}{f_y}\right)^2 + \left(\frac{\sigma_h}{f_y}\right)^{2\eta} - 2\nu\frac{\sigma_a}{f_y}\frac{\sigma_h}{f_y} = 1.0 \tag{4}$$

in which

σ_a, σ_h	axial and circumferential (hoop) stresses, respectively, tensile positive,
f_y	yield strength,
ν	Poisson's ratio (= 0.3).
η	factor introduced to reduce the conservatism in elastic results for tubulars loaded in tension.

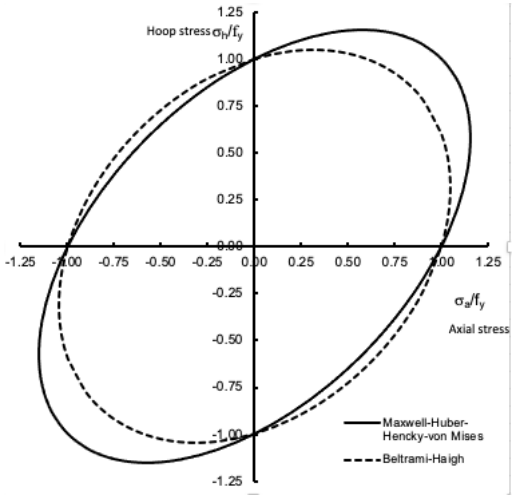

FIGURE 1: COMPARISON OF BELTRAMI-HAIGH AND MISES YIELD FUNCTIONS

Taking the first term in Equation (4) to represent bending, i.e. σ_b/f_b where f_b is the ISO 19902 bending strength, and the second term to represent hoop condition, i.e. σ_h/f_h where f_h is the ISO 19902 hoop buckling strength, assuming the bending stress is tensile, since hoop stress is negative, the sign of the third term becomes positive for consistency with the ISO 19902 presumption that, in code check formulae, all stresses are taken as positive irrespective of their actual sign. Treating Equation (4) as a quadratic and solving for the first term, gives:

$$\frac{\sigma_b}{f_b} = \sqrt{1.0 + 0.09\left(\frac{\sigma_h}{f_h}\right)^2 - \left(\frac{\sigma_h}{f_h}\right)^{2\eta}} - 0.3\frac{\sigma_h}{f_h} \tag{5}$$

Introducing B in place of σ_h/f_h and realising that σ_b is the maximum bending stress in the presence of pressure, i.e., $f_{b,h}$, leads to ISO 19902:2020 Formula (13.4-9), i.e.

$$f_{b,h} = f_b\left(\sqrt{1.0 + 0.09B^2 - B^{2\eta}} - 0.3B\right) \tag{6}$$

with $\eta = 5 - 4\frac{f_h}{f_y}$, i.e. ISO 19902:2020 Formula (13.4-11).

Figure 2 plots Equation (6) with hoop compression positive and bending tension negative, for η values from 1-5, the test range of η. Values of η =1.0 imply stocky sections while 5.0 imply very slender cross-sections or long unstiffened tubulars, or both. As η increases, the curve expands, more so for pressure than for bending, this trend indicating a growing independence for elastic buckling conditions.

A major problem with Equation (6) is that many test results have values of B > 1.0 for which it has no solution. Clearly when performing code checks, the same problem can arise when seeking to converge to a solution.

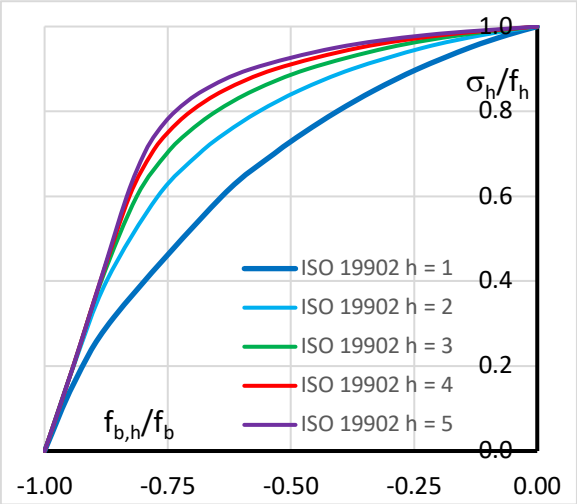

FIGURE 2: EFFECT OF η ON ISO 19902 BENDING STRENGTH - PRESSURE INTERACTION

The main problem with this formula, when combined with axial compression, is that it is particularly conservative with respect to test data can be seen from Figures 3(a) and (b). Here the modelling uncertainty parameter X_{m}, i.e. ratio of test to predicted value, is plotted with respect to model number, 69 for the local buckling database and 26 for the column buckling database: when calculating X_{m}, all partial resistance factors are set to unity. Overall statistics for X_{m} are given bottom right while the statistics for each failure mode are listed in the key together with two subsets of the data, zero bending stress and zero axial stress conditions.

Four failure modes are possible: hoop buckling; local compression, bending and pressure; column buckling, bending and pressure; and elastic buckling. Because ISO 19902 requires hoop buckling to be checked first, the hoop buckling data included in the figures is either because their X_{m} value was greater than unity or they were the largest X_{m} over all failure modes. Both hoop buckling datasets are only slightly conservatively predicted as is the elastic buckling data of Figure 3 (a). In contrast, both local and column buckling data are significantly under-estimated with biases 25% more than parity.

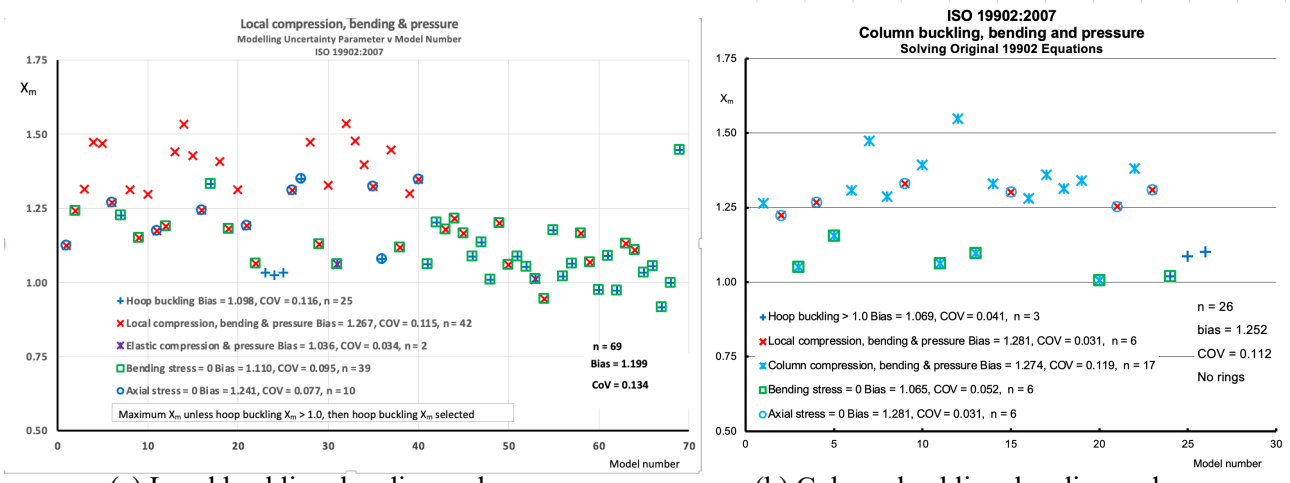

(a) Local buckling, bending and pressure (b) Column buckling, bending and pressure

FIGURE 3: X_{m} FOR ISO 19902:2007 STRENGTH FORMULATIONS

The relatively low biases registered for the zero bending stress condition compared with those for local and column buckling indicate Equation (6) is conservative when bending is involved. The high bias for when axial stress is zero confirms this although these particular models could also be checked under combined tension, bending and pressure.

EFFECT OF ISO 19902:2020 CHANGES

The only relevant change to the tubular member strength formulations in ISO 19902 2nd edition was to replace the linear interaction between local axial and bending, Equations (1) and (2), by a cosine interaction, i.e.

$$1 - \cos\left(\frac{\pi}{2}\frac{\gamma_{\mathrm{R,t}}\sigma_{\mathrm{t,c}}}{f_{\mathrm{t,h}}}\right) + \frac{\gamma_{\mathrm{R,b}}\sigma_{\mathrm{b}}}{f_{\mathrm{b,h}}} \leq 1.0 \tag{7}$$

$$1 - \cos\left(\frac{\pi}{2}\frac{\gamma_{\mathrm{R,c}}\sigma_{\mathrm{c,c}}}{f_{\mathrm{yc}}}\right) + \frac{\gamma_{\mathrm{R,b}}\sigma_{\mathrm{b}}}{f_{\mathrm{b,h}}} \leq 1.0 \tag{8}$$

The effect on the X_{m} comparisons is reflected in Figures 4 (a) and (b) noting that, when checking Equation (8), values of $\sigma_{\mathrm{c,c}}/f_{\mathrm{yc}} > 1.0$ with $\gamma_{\mathrm{R,c}} = 1.0$ are invalid so the term is simply replaced by $\sigma_{\mathrm{c,c}}/f_{\mathrm{yc}}$. Given the more accurate equation for local buckling/bending interaction, the reduction in biases for local buckling bending and pressure, compared with the results in Figure 3, of over 5% in (a) and 10% in (b) is expected. Because the local buckling formulation is now less conservative, for the column buckling condition in (b), local buckling governs the failure of more models than for the 2007 version, 12 instead of 6, with a commensurate reduction in models governed by column buckling, this has led to a 4% reduction in the column buckling bias. Both overall biases reduced a similar amount.

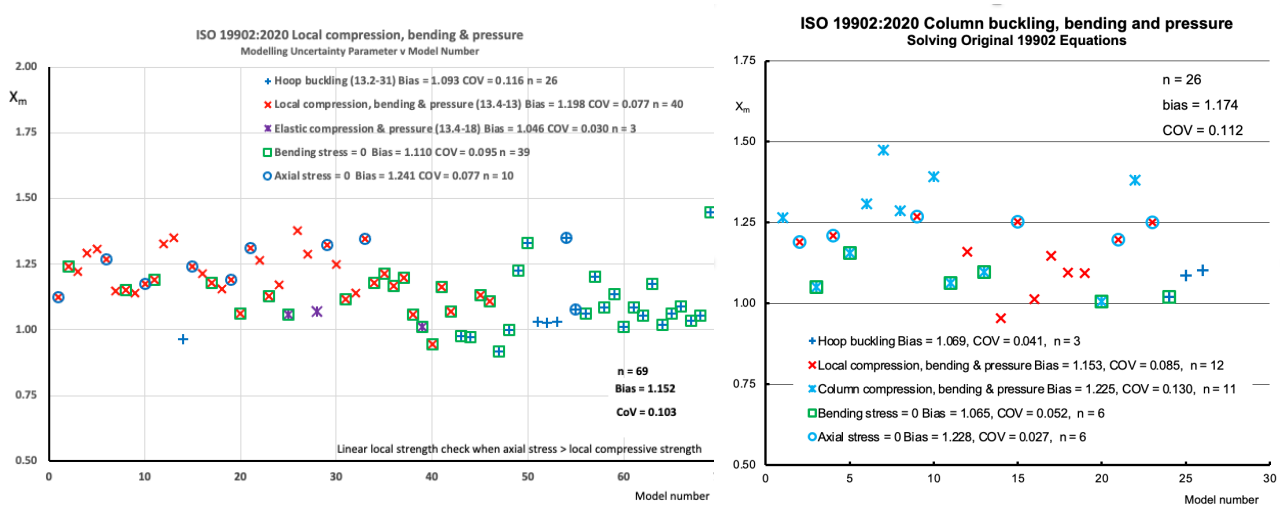

(a) Local buckling, bending and pressure (b) Column buckling, bending and pressure

FIGURE 4: X_m FOR ISO 19902:2020 STRENGTH FORMULATIONS

DIRECT SOLUTION OF THE BELTRAMI-HAIGH YIELD FUNCTION

If $f_{b,h}$ in Equations (2) and (8) is replaced by the Beltrami-Haigh function, i.e. Equation (4), Equations (9) and (10) are realised assuming bending and hoop stresses are of opposite signs with $X_{m,l}$ and $X_{m,c}$ representing the modelling uncertainty parameters for local buckling and column buckling, respectively.

$$1 - \cos\left(\frac{\pi}{2}\frac{\sigma_{c,c}}{f_{yc}\,X_{m,l}}\right) + \sqrt{\left(\frac{\sigma_b}{f_b\,X_{m,l}}\right)^2 + \left(\frac{\sigma_h}{f_h\,X_{m,l}}\right)^{2\eta} + 2\nu\frac{\sigma_b}{f_b\,X_{m,l}}\frac{\sigma_h}{f_h\,X_{m,l}}} \tag{9}$$

$$\frac{\sigma_c}{f_{c,h}\,X_{m,c}} + \sqrt{\left(\frac{1}{f_b}\left(\frac{\sigma_b/X_{m,c}}{1-\sigma_c/(X_{m,c}f_e)}\right)\right)^2 + \left(\frac{\sigma_h}{f_h\,X_{m,c}}\right)^{2\eta} + 2\nu\frac{1}{f_b}\left(\frac{\sigma_b/X_{m,c}}{1-\sigma_c/(X_{m,c}f_e)}\right)\frac{\sigma_h}{f_h\,X_{m,c}}} \tag{10}$$

Figure 5 presents the resulting comparisons with test data. For (a) local buckling, all biases have increased, except for the zero axial stress condition, most notably local buckling 9.5% and zero bending stress condition 13%. For (b) column buckling, notable increases include column buckling 10.8% and local buckling 6.7% while the zero bending stress condition has increased 9.3%. Also the maximum X_m increased in both cases, for (a) up significantly from 1.45 to 1.83. All of these indicate considerable conservatism in these formulations.

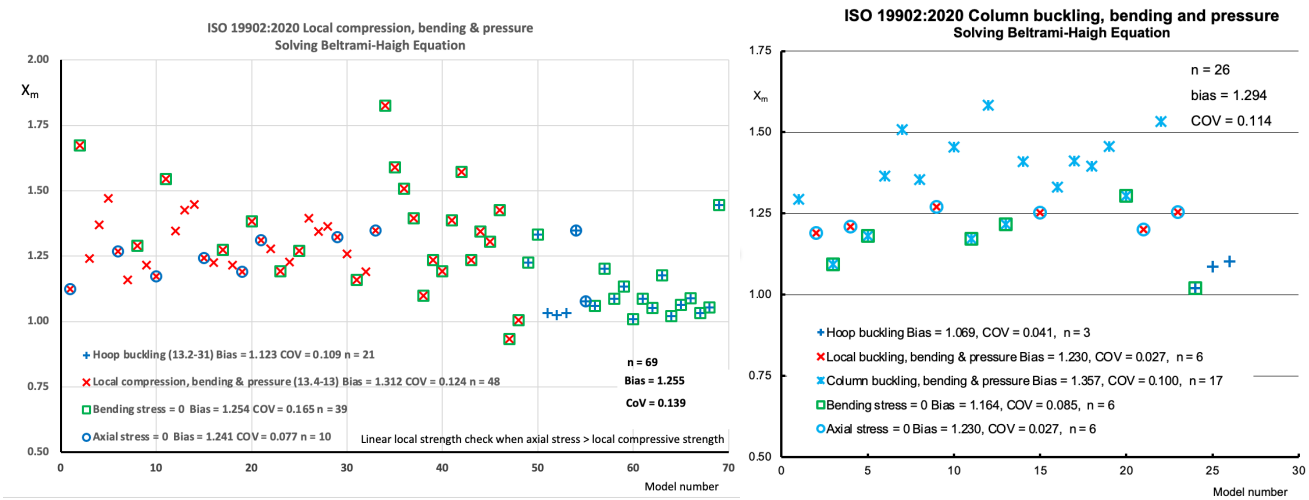

(a) Local buckling, bending and pressure (b) Column buckling, bending and pressure

FIGURE 5: X_m FOR BELTRAMI-HAIGH VERSIONS OF ISO 19902:2020

A feature of the existing bending-pressure interaction is that it assumes the stresses are of opposite sign, i.e. bending stress is tensile so the formulation is based on the +/- quadrant of the Beltrami-Haigh yield function.

In the presence of significant axial compression and little bending, the dominant axial stress is compressive so failure is more likely in the -/- quadrant. This is considered in the next section, however, for consistency with the ISO 19902 convention that all stresses are taken to be positive, taken as the +/+ quadrant.

SOLUTION OF THE BELTRAMI-HAIGH YIELD FUNCTION IN +/+ QUADRANT

The relevant equations are almost identical to Equations (9) and (10) but with a change of sign to the third term under the square root sign, i.e.,

$$1 - \cos\left(\frac{\pi}{2}\frac{\sigma_{c,c}}{f_{yc}\,X_{m,l}}\right) + \sqrt{\left(\frac{\sigma_b}{f_b\,X_{m,l}}\right)^2 + \left(\frac{\sigma_h}{f_h\,X_{m,l}}\right)^{2\eta} - 2\nu\frac{\sigma_b}{f_b\,X_{m,l}}\frac{\sigma_h}{f_h\,X_{m,l}}} \tag{11}$$

$$\frac{\sigma_c}{f_{c,h}\,X_{m,c}} + \sqrt{\left(\frac{1}{f_b}\left(\frac{\sigma_b/X_{m,c}}{1-\sigma_c/(X_{m,c}f_e)}\right)\right)^2 + \left(\frac{\sigma_h}{f_h\,X_{m,c}}\right)^{2\eta} - 2\nu\frac{1}{f_b}\left(\frac{\sigma_b/X_{m,c}}{1-\sigma_c/(X_{m,c}f_e)}\right)\frac{\sigma_h}{f_h\,X_{m,c}}} \tag{12}$$

Figure 6 presents the resulting comparisons with test data. For (a), there is no change to hoop buckling because this check is outside the Beltrami-Haigh function and local compression, bending and pressure is down nearly 10% mainly due to change in sign of bending. The zero bending condition is unchanged because axial compression is outside the Beltrami-Haigh function while, for the zero axial stress condition, the bias is down 17.6% because bending is no longer quantified conservatively. For (b), again no change to hoop buckling while local compression, bending and pressure is down nearly 26% to 0.913 but none are subject to axial loading so would need to be checked using the tension, bending and pressure formulation. The column compression, bending and pressure bias is down some 16% while the zero bending condition is again unchanged and the zero compression condition is down 22.5%.

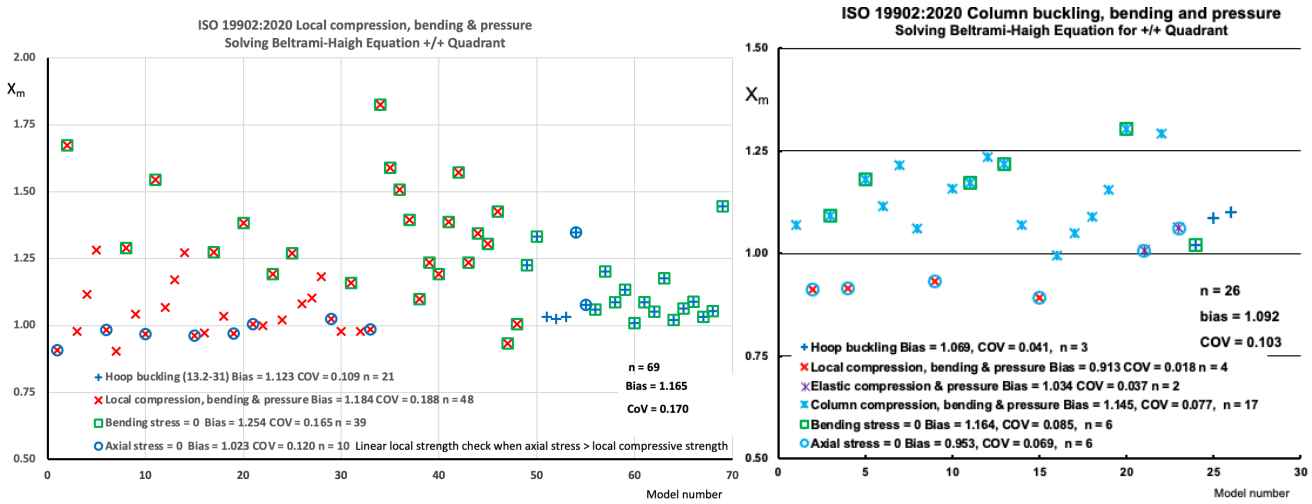

(a) Local buckling, bending and pressure (b) Column buckling, bending and pressure

FIGURE 6: X_m FOR BELTRAMI-HAIGH VERSIONS OF ISO 19902:2020 +/+ QUADRANT

In Equations (11) and (12), the compression and bending terms are now of the same sign. Since the local compression, bending and pressure formulation, in particular, is a strength check, there is no reason why the compression terms cannot be included in the Beltrami-Haigh yield function, i.e.

$$\sqrt{\left(\left[1 - \cos\left(\frac{\pi}{2}\frac{\sigma_{c,c}}{f_{yc}\,X_{m,l}}\right)\right] + \frac{\sigma_b}{f_b\,X_{m,l}}\right)^2 + \left(\frac{\sigma_h}{f_h\,X_{m,l}}\right)^{2\eta} - 2\nu\left(\left[1 - \cos\left(\frac{\pi}{2}\frac{\sigma_{c,c}}{f_{yc}\,X_{m,l}}\right)\right] + \frac{\sigma_b}{f_b\,X_{m,l}}\right)\frac{\sigma_h}{f_h\,X_{m,l}}} \tag{13}$$

$$\sqrt{\left(\frac{\sigma_c}{f_{c,h}\,X_{m,c}} + \frac{1}{f_b}\left(\frac{\sigma_b/X_{m,c}}{1-\sigma_c/(X_{m,c}f_e)}\right)\right)^2 + \left(\frac{\sigma_h}{f_h\,X_{m,c}}\right)^{2\eta} - 2\nu\left(\frac{\sigma_c}{f_{c,h}\,X_{m,c}} + \frac{1}{f_b}\left(\frac{\sigma_b/X_{m,c}}{1-\sigma_c/(X_{m,c}f_e)}\right)\right)\frac{\sigma_h}{f_h\,X_{m,c}}} \tag{14}$$

Figure 7 presents the resulting comparisons with test data. For (a), hoop buckling is reduced by 2% while local compression, bending and pressure is down 12.5% to 1.035, the most accurate of all the comparisons. The zero

bending condition has reduced by 14% to 1.082, also lower than any of the previous comparisons. The zero axial compression condition is unchanged at 1.023, expected because the relevant stress combination is unaffected. For (b), both hoop buckling and local compression, bending and pressure are unchanged. Column compression, bending and pressure is down 7.5% to 1.059, the most accurate of all the comparisons. The zero bending stress condition has reduced to 0.957 while the zero compression condition is unchanged.

Overall biases of 1.059 and 1.036 for (a) and (b), respectively, are indicative of relatively unbiased sets of criteria, while CoVs have fallen below 10% for the first time which, taken together, confirm the selection of reasonably accurate strength formulations.

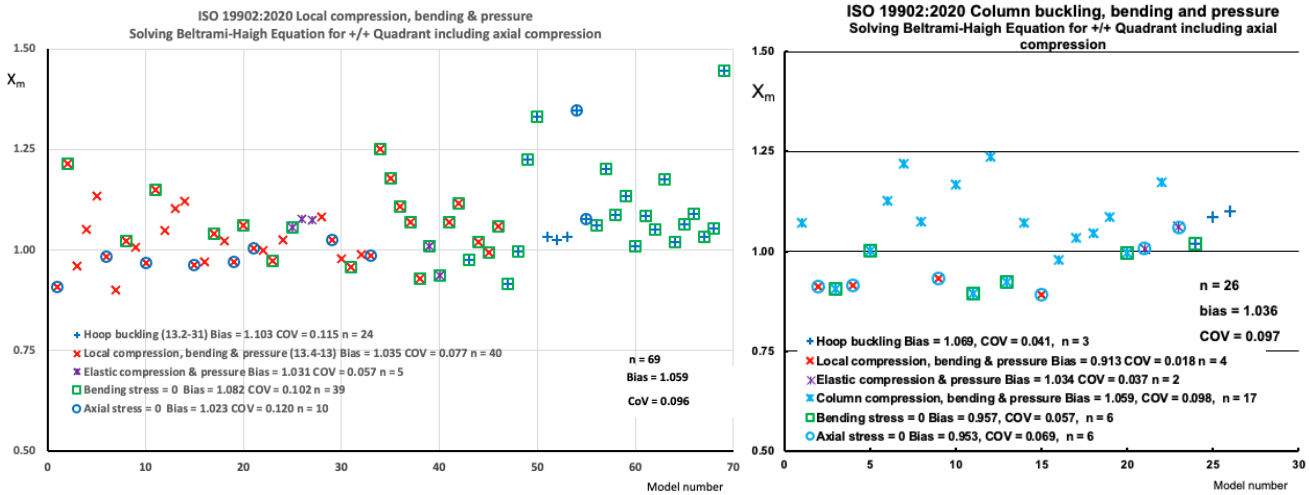

(a) Local buckling, bending and pressure (b) Column buckling, bending and pressure

FIGURE 7: X_m FOR BELTRAMI-HAIGH VERSIONS OF ISO 19902:2020 INCORPORATING COMPRESSION TERMS +/+ QUADRANT

One question that arises in relation to the column compression strength formulation is that it already contains a pressure term so, are the present set of criteria counting the effect of pressure twice. Column compression strength, $f_{c,h}$, is given by ISO 19902:2020 Formulae (13.4-15) and (13.4-16), namely:

$$f_{c,h} = \frac{1}{2} f_{yc} \left[(1.0 - 0.278\lambda^2) - \frac{2\sigma_q}{f_{yc}} + \sqrt{(1.0 - 0.278\lambda^2)^2 + 1.12\lambda^2 \frac{\sigma_q}{f_{yc}}} \right] \quad \text{for } \lambda \le 1.34 \sqrt{\left(1 - \frac{2\sigma_q}{f_{yc}}\right)^{-1}} \qquad (15a)$$

$$f_{c,h} = \frac{0.9}{\lambda^2} f_{yc} \quad \text{for } \lambda > 1.34 \sqrt{\left(1 - \frac{2\sigma_q}{f_{yc}}\right)^{-1}} \qquad (15b)$$

in which

$\lambda = \sqrt{\frac{f_{yc}}{f_e}}$ column slenderness parameter,

f_e Euler buckling strength,

σ_q capped-end stress, introduced to reflect the fact that it does not cause column buckling although it can contribute to yielding.

The effect of capped-end stress on column strength is seen in Figure 8 in which $f_{c,h}$ is plotted against λ for a tubular member with a yield strength of 350 MPa and a diameter to thickness ratio of 40 for water depths up to 500 m. Each 100 m of depth equates to a capped-end stress of 10.05 N/mm^2. As this is an axial stress, it can be seen to simply reduce the available axial capacity by an equivalent amount so that, at 500 m, the effective yield strength is 350 – 50.25 = 299.75 N/mm^2 as can be appreciated from Figure 8 when λ is 0. It is also seen from the figure that, as expected, elastic column buckling strength is not affected by pressure.

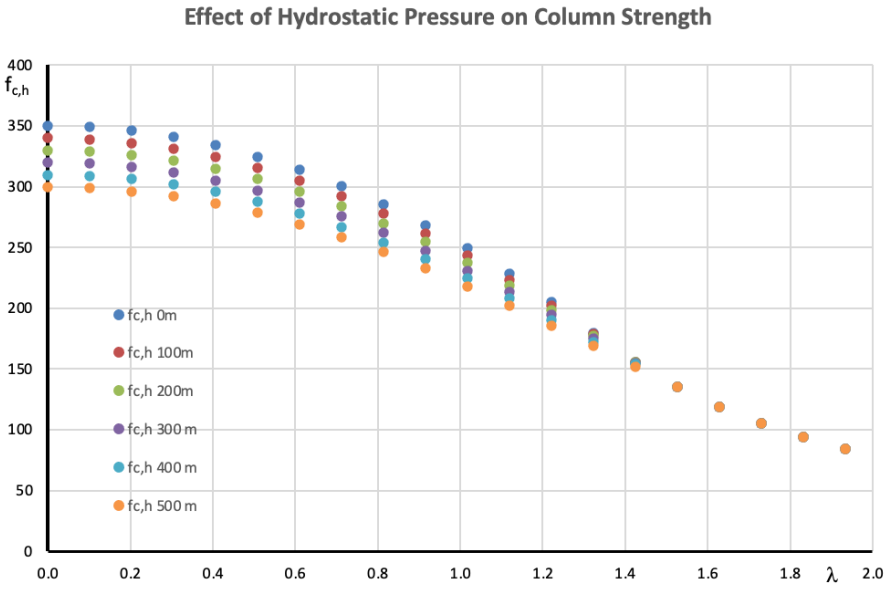

FIGURE 8: ISO 19902:2020 FORMULAE (13.4-15 & 16) - EFFECT OF WATER DEPTH

A further demonstration that the capped-end stress is equivalent to reducing yield strength can be found in the results presented in Table 1. Four test specimens in the column buckling database, model numbers 3, 5, 11 and 13, were subjected to compression and pressure only, i.e. no bending. So, their X_ms can be determined using the ISO 19902 column strength equations in the absence of pressure, i.e. Formulae (13.2-5) and (13.2-6):

$$f_c = (1.0 - 0.278\lambda^2) f_{yc} \qquad \text{for } \lambda \leq 1.34 \tag{16a}$$

$$f_c = \frac{0.9}{\lambda^2} f_{yc} \qquad \text{for } \lambda > 1.34 \tag{16b}$$

Since the effect of pressure has been removed, column strengths are higher than previously, so their X_ms should be lower, as confirmed by the values listed in columns 2 and 3 of Table 1. If Equations (16a) and (16b) are recalculated with f_{yc} replaced by $f_{yc,e} = f_{yc} - \sigma_q$, i.e. yield strength reduced by the capped-end stress, the outcomes are listed in column 4. If the postulate that the capped-end stress simply reduces yield strength is valid, then a similar result to that in column 3 should be achieved. The column 3 to the column 4 ratios are listed in the final column and can be seen to lie within 2.5% which seems to confirm the postulate.

TABLE 1: COMPARISON OF COLUMN X_m

Model	X_m, f_c	X_m, $f_{c,h}$	X_m, f_c based on $f_{yc,e}$	X_m $f_{c,h}/(X_m, f_y$ based on $f_{yc,e})$
3	0.836	0.906	0.891	1.017
5	0.960	1.002	0.993	1.009
11	0.843	0.894	0.874	1.023
13	0.875	0.923	0.911	1.013

On the basis of the above, Equations (13) and (14) have been proposed to replace ISO 19902:2020 Formulae (13.4-13) and (13.4-14) in the next edition. As they offer less conservatism than the existing formulations, they are used in the next section to derive a revised ISO 19905-1 Table A.12.5-1.

DERIVING A REPLACEMENT ISO 19905-1 TABLE A.12.5-1

For ISO 19902 next edition, Equations (13) and (14) will govern compression, bending and hydrostatic pressure combinations while Equation (7) will govern tension, bending and hydrostatic pressure combinations. These equations have been subject to a parametric study to cover the likely combination of tubulars that might be used in practice. Hoyle [5] provided the relevant data for D/t and L/D (length/diameter) ratios and yield strengths. Figure 9 is a plot of the data showing maximum D/t ratios are around 35 and maximum L/D ratios

are nearly 40. In the existing Table A.12.5-1, D/t ratios up to 60 were listed so the parametric study covered D/t ratios of 10, 20, 30 , 40 , 50 and 60 and L/D ratios of 15, 30 and 45. From [5], yield strength ranged from 353 MPa to 784.5 MPa. For the study, yield strengths of 450 MPa, 650 MPa and 850 MPa were considered. Since Table A.12.5-1 is presented in terms of head of water, the study used water depth and not pressure as a determining parameter.

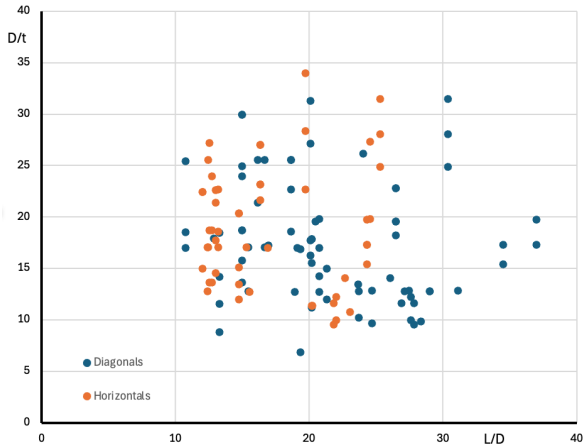

FIGURE 9: TYPICAL JACK-UP TUBULAR MEMBER D/t AND L/D RATIOS

The objective of the study was, as previously, to determine the water depth that causes a 10% reduction in strength. For compression, this was effected by determining the local or column buckling strength in the absence of pressure, then calculating the water depth to reduce the strength to 90% of this value recalling that for local buckling, the capped-end stress is added to the applied compressive stress and that for column buckling, the capped-end stress effectively reduces the yield strength. When applying bending, a similar approach is adopted but the capped-end stresses that develop means that a nominally bending-pressure condition has to be checked for combined compression, bending and pressure. For the tension only condition, the applied tension is reduced by the capped-end stress which, when D/t = 10, equates to a stress equal to 1/3rd of yield strength while when D/t = 60, the capped-end stress is only 2.5% of yield. When examining bending with tension interaction, Equation (7), a tensile stress equal to the capped-end stress is applied to ensure the check does not default to a bending-compression check.

Examination of the governing equations indicates those involving tension, local compression and bending are independent of length while column buckling and hoop buckling are length dependent, the latter through the parameter $\mu = (L/D)\sqrt{2D/t}$ which determines the value of the elastic hoop buckling coefficient. This length dependency can be seen in Figure 10 versus D/t as a function of water depth and yield strength. Each failure mode was checked for nominally pure compression, pure tension and pure bending within the constraints of stress combinations discussed above. Closer examination shows yield strength to be important but only for D/t ratios less than about 30. This is a consequence of the relatively large μ values that arise from the combination of L/D and D/t parameters under consideration which leads to hoop buckling strengths being equal to the elastic critical buckling stress for D/t ratios from 30 to 60.

The water depth ranges shown in Figure 10 fall well outside the range covered in Table A.12.5-1 of up to 200 m. Useful as Figure 10 is in providing insight into the influence of all geometrical and material properties on tubular member strength, the depth needs to be limited for the purpose of creating a new version of the table. Figure 11 shows the same figures but with depth limited to 600 m. Figure 11 a) exhibits the lowest pressure capability and, of these, bending combined with capped-end tension is the most affected by pressure while also being independent of yield strength and L/D.

Table 2 lists the water depths and D/t values corresponding to this set of curves. Excel Solver was used to provide a best fit to these values using the same form of equation as the existing, as follows:

$$d_{\mathrm{w,lim}} = \left(\frac{233}{D/t}\right)^{2.999} \tag{17}$$

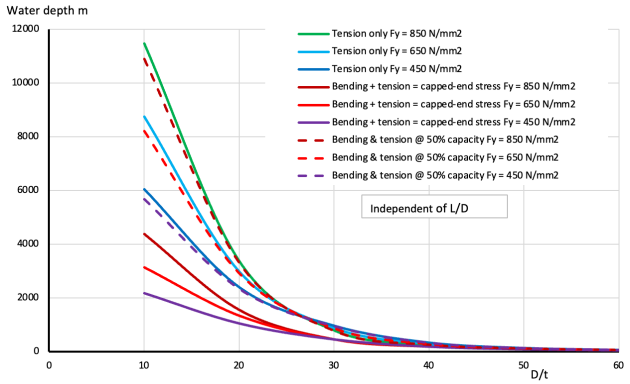

a) Tension and bending

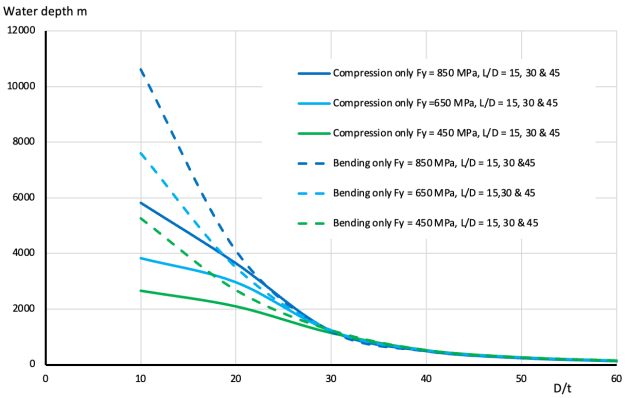

b) Local compression and bending

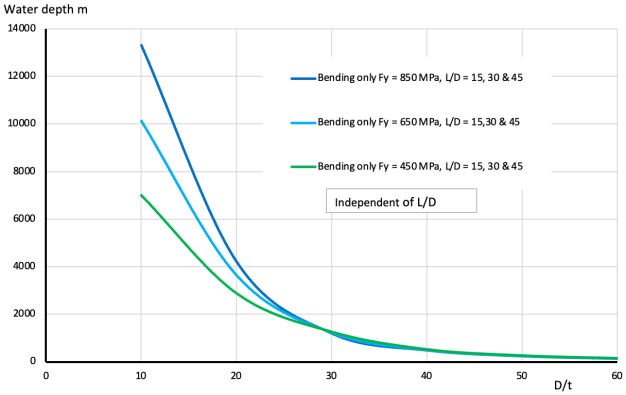

c) Columns under bending only

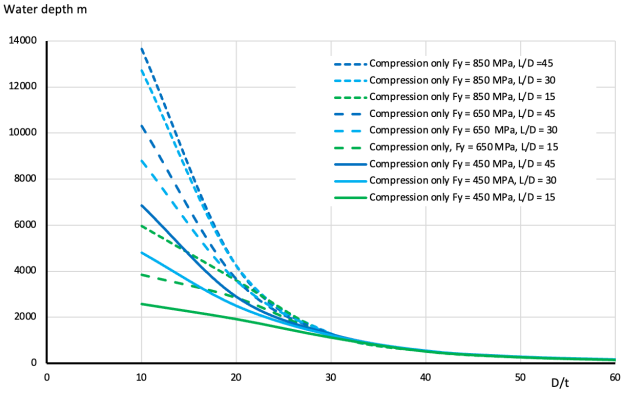

d) Columns compression only

FIGURE 10: EFFECT OF WATER DEPTH, D/t, L/D AND YIELD STRENGTH ON TUBULAR MEMBER STRENGTH

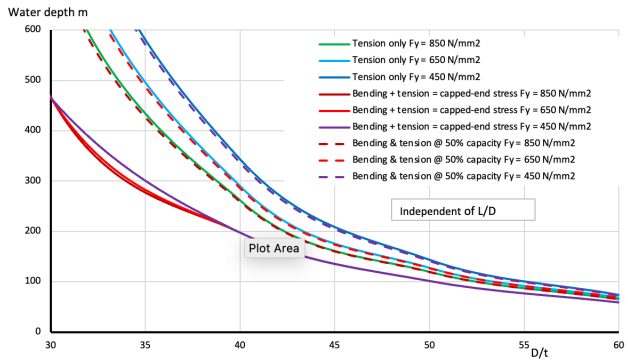

a) Tension and bending

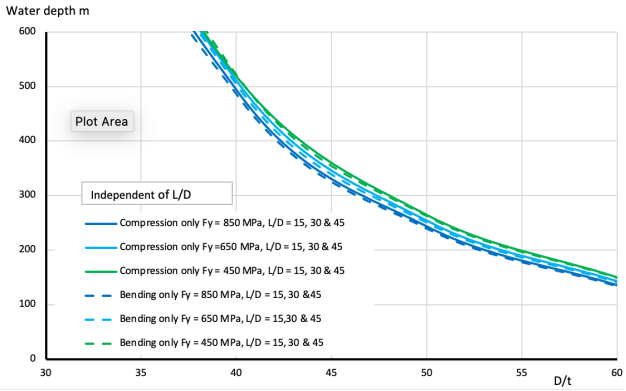

b) Local compression and bending

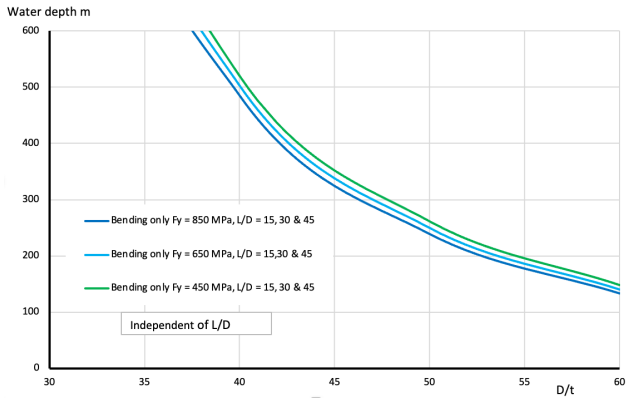

c) Columns under bending only

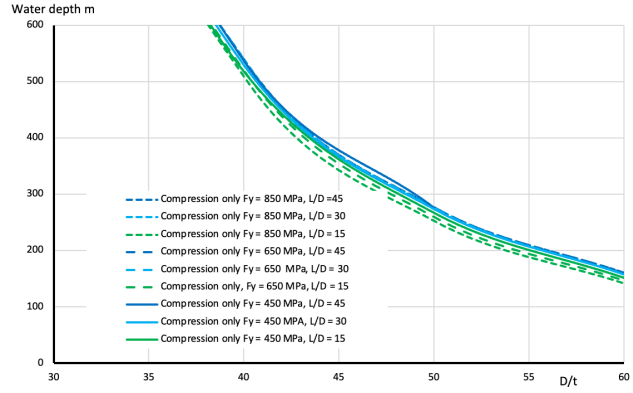

b) Columns compression only

FIGURE 11: EFFECT OF WATER DEPTH UP TO 600 m, D/t, L/D AND YIELD STRENGTH ON TUBULAR MEMBER STRENGTH

TABLE 2: MINIMUM CALCULATED WATER DEPTHS GIVEN D/t

D/t	Calculated water depth (m)
30	465.46
40	197.32
50	101.10
60	58.50

Equation (17) has been used to create Table 3, apart from the first entry which comes directly from Table 2, for virtually the same range of water depths as in the current version of Table A.12.5.-1. It is proposed as the replacement for the existing version.

TABLE 3: REPLACEMENT TABLE A.12.5-1

Equivalent head of water $d_{w,lim}$ (m)	Maximum tubular D/t
58.5	60.0
75	55.2
100	50.2
125	46.6
150	43.8
200	39.8

CONCLUSION

The tubular member strength formulations in ISO 19905-1 Site-specific assessment of Jack-ups are based those developed for ISO 19902 Fixed steel offshore structures. ISO 19905-1 Table A.12.5-1 tabulates limiting tubular member D/t ratios for water depths up to 200 m for which the effects of hydrostatic pressure can be ignored: the table was based on a draft of ISO 19902:2007. ISO 19902:2020 contains modified tubular member strength formulations and further changes are now proposed for the next edition, expected 2027. Both the 2020 and the proposed changes are relevant to jack-up assessment. It was thus considered timely to assess the effects of these changes on Table A.12.5-1.

Both sets of ISO 19902 changes have been examined in detail and the formulation governing the water depth limit given D/t identified: it is found to be independent of yield strength and L/D ratio. It has been used to revise the formula for the limiting water depth given D/t ratio. A replacement Table A.12.5-1 is presented in Table 3. The limiting tubular D/t ratios have all increased by 11%.

ACKNOWLEDGEMENT

Mike Hoyle Noble Denton Marine Services DNV is gratefully acknowledged for providing data on typical jack-up tubular member yield strengths and L/D and D/t ratios, the geometrical parameters are summarised in Figure 9 of the paper.

REFERENCES

[1] PAFA Consulting Engineers. ISO/TC 67/SC 7/WG 7/Panel 10 Structural strength acceptance criteria, Final Report to Health and Safety Executive, C071-065-R Rev 1, March 2002.
[2] Frieze PA. ISO 19902 Tubular members including damaged and grouted Members, Proceedings 30th International Conference on Ocean, Offshore and Arctic Engineering, OMAE2011, Rotterdam, June 2011, OMAE2011-50106.
[3] Ku A, Richmond M. American and European hydrostatic tubular beam-column equation comparisons, Journal of Offshore Mechanics and Arctic Engineering, August 2023, Vol. 145, 041703.
[4] Frieze PA. Note on ISO 19902:2020 Clause 13.4.3 Tubular members subject to axial compression, bending and hydrostatic pressure effects, Note to ISO/TC 67/SC 7/WG 3, 27 May 2025.
[5] Hoyle M. Jack-up brace info. Private communication, 5 September 2025.